Fluctuating arrivals of short-range acoustic data

Cheolsoo Park
Maritime and Ocean Engineering Research Institute (MOERI), Daejeon 305-343, Korea

Woojae Seong[a)]
Department of Ocean Engineering, Seoul National University, Seoul 152-744, Korea

Peter Gerstoft and William S. Hodgkiss
Marine Physical Laboratory, University of California San Diego, 9500 Gillman Drive, La Jolla, California 92093

(Received 7 January 2010; revised 11 October 2010; accepted 12 October 2010)

Geoacoustic inversion using fluctuating signal observations can be challenging. The origin of these fluctuations needs to be understood so the signals can be used appropriately. A set of experiments [Tang *et al*., Oceanogr. **20**(4), 156–167 (2007)] was carried out in shallow water near the New Jersey shelf break in summer 2006. Significant fluctuations in the direct path and surface-reflected arrivals of short-range chirp transmissions (1.1–2.9 kHz) were observed on a vertical line array. This paper explains the origin of these signal fluctuations through analysis of the arrival amplitudes. It is shown that the strong thermocline combined with an oscillating source motion due to ocean surface waves results in the signal fluctuations. © *2011 Acoustical Society of America.*
[DOI: 10.1121/1.3514505]

PACS number(s): 43.30.Pc, 43.60.Jn [AIT] Pages: 98–103

I. INTRODUCTION

For geoacoustic inversion, a stable received signal usually is required to obtain stable inversion results. When using fluctuating acoustic data for inversion, first it is important to understand the fluctuations so that the signals can be used appropriately. The acoustic field depends on the ocean environment (including water column, bottom, and surface) and on the source–receiver configuration. As at least one of these factors varies, the acoustic data will exhibit corresponding variations. The time scale of temporal variation ranges widely from seconds to days depending on the factors such as ocean surface waves, internal waves, fronts, eddies, and tides. Among them, the seconds-scale variation clearly is visible in broadband acoustic data, especially when the source repeatedly emits high frequency (>1 kHz) signals. Often, the acoustic data fluctuations affect the data application adversely. Thus, it is desirable that the origin of these temporal variations be understood.

A set of experiments (Shallow Water 2006, SW06) was carried out in shallow water near the New Jersey shelf break in summer 2006.[1] Significant fluctuations in direct and surface-reflected arrival amplitudes of short-range chirp transmissions (1.1–2.9 kHz) were observed on a vertical line array (VLA). The source followed a circular path around the vertical array with mean radius 198 m on September 3, 2006, the day after tropical storm Ernesto passed through the experimental area. More stable short-range signals were observed near this site prior to Ernesto and were used in the analysis in Refs. 2–4. Here, the relationship between signal fluctuations and the ocean surface waves after the storm is studied in detail. It is demonstrated that these fluctuations are due to the strong thermocline at the site combined with source-depth oscillations due to ocean surface waves.

II. EXPERIMENT DESCRIPTION

The experiment was performed near the New Jersey continental shelf break. Acoustic data were recorded on an L-shaped line array (SWAMI32) located at (39° 3.618'N, 73° 7.897'W).[5] The SWAMI32 VLA consisted of ten hydrophones with 5.95 m spacing. The bathymetry is range-independent with water depth of 69 m. According to the surveys in the vicinity, the seabed consists of a coarse sand ridge above the outer shelf wedge of a sand–clay–silt mixture.[5,6]

During the experiment, R/V Knorr towed a source at 0.5–1 knots along the circular track around the VLA, see Fig. 1(a). Based on a global positioning system (GPS) mounted on the stern near the source, the mean radius was 198 m with 7 m standard deviation. The circle event started at 22:50 UTC (Coordinated Universal Time) and finished at 24:20 UTC on September 3, 2006. The source was at about 35 m depth and emitting a 1-s linear frequency modulation (LFM) transmission swept from 1.1 to 2.9 kHz every second.

Along with acoustic data acquisition, environmental data were measured at the site. A conductivity–temperature–depth (CTD), see Fig. 1(b), was taken near SWAMI32 during this experiment (CTD44, 21:56 UTC, 39° 3.610'N, 73° 8.010'W). In the sound speed profile (SSP), a pronounced thermocline at 25 m depth (near channel 3) is observed and a weaker thermocline is formed deeper. Strong swell was observed at the experimental site. Figure 1(c) shows the spectral energy density of ocean waves measured for 30 min on the air–sea interaction spar (ASIS) buoy[7] located 8.2 km from the VLA. According to this spectrum, the ocean surface waves peak frequency was 0.12 Hz and the significant wave

[a)]Author to whom correspondence should be addressed. Electronic mail: wseong@snu.ac.kr

 0001-4966/2011/129(1)/98/6/$30.00

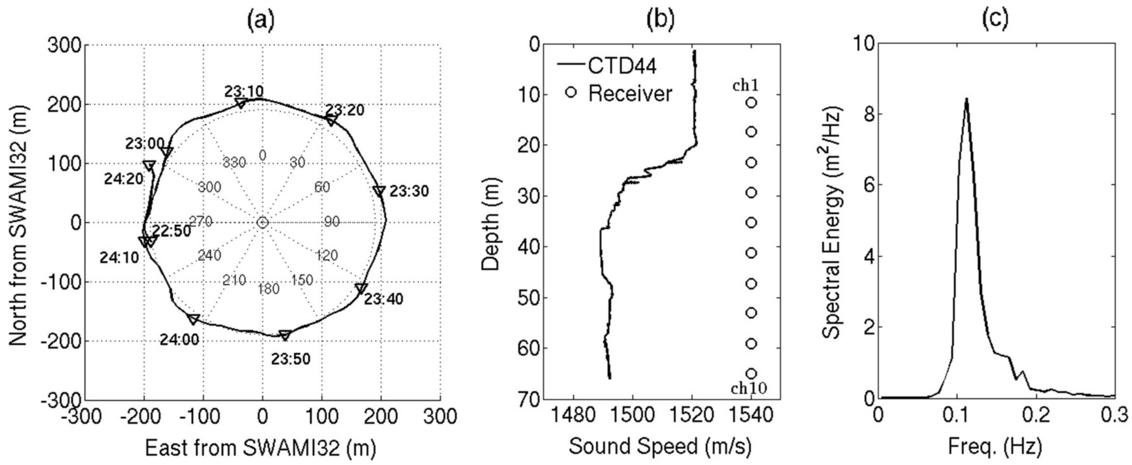

FIG. 1. Experiment and environment. (a) Source trajectory with respect to the SWAMI32 VLA with position (∇) at selected times. Angles (°) relative to North are given inside the circle with mean radius 198 m. (b) Sound speed profile from CTD44 (21:56 UTC) with receiver positions (o). (c) The surface wave spectrum from 24:19 to 24:49 UTC on the ASIS buoy.

height was estimated as 2.2 m.[8] From the two-dimensional (2D) ASIS spectrum, the dominant wave direction was 90° ± 40°.

III. ACOUSTIC DATA FLUCTUATION ANALYSIS

A. Analysis of the arrival amplitudes

The data obtained from ten hydrophones on the SWAMI32 VLA were analyzed. The raw data were matched filtered using a synthetic 1-s 1.1–2.9 kHz LFM waveform. Figure 2(a) shows an example of the matched filtered time series for all channels, shown without any time alignment. Due to the wavelet being compressed after matched filtering and the short source–VLA distances (198 m), a well-resolved arrival structure including D, SR, and BR arrivals is obtained. The experimental site was on the sand ridge above the outer shelf wedge (see Sec. II). The thickness of the sand layer was 3–5 m.[5] However, the sub-bottom reflection is not evident in the data which might be due to the lower impedance contrast between the sand layer and outer shelf wedge compared to the water–seabed interface.

All of the experimental data showed similar arrival structure as Fig. 2(a). However, the amplitude and the travel time (phase) of each arrival vary across pings as shown in Fig. 2(b) for channel 3 based on 380 pings (380 s, covering a 20° portion of the circle) starting at 22:50 UTC. The large, slow variation in travel time is due to the source–VLA range variation as the source went around in the circle. All

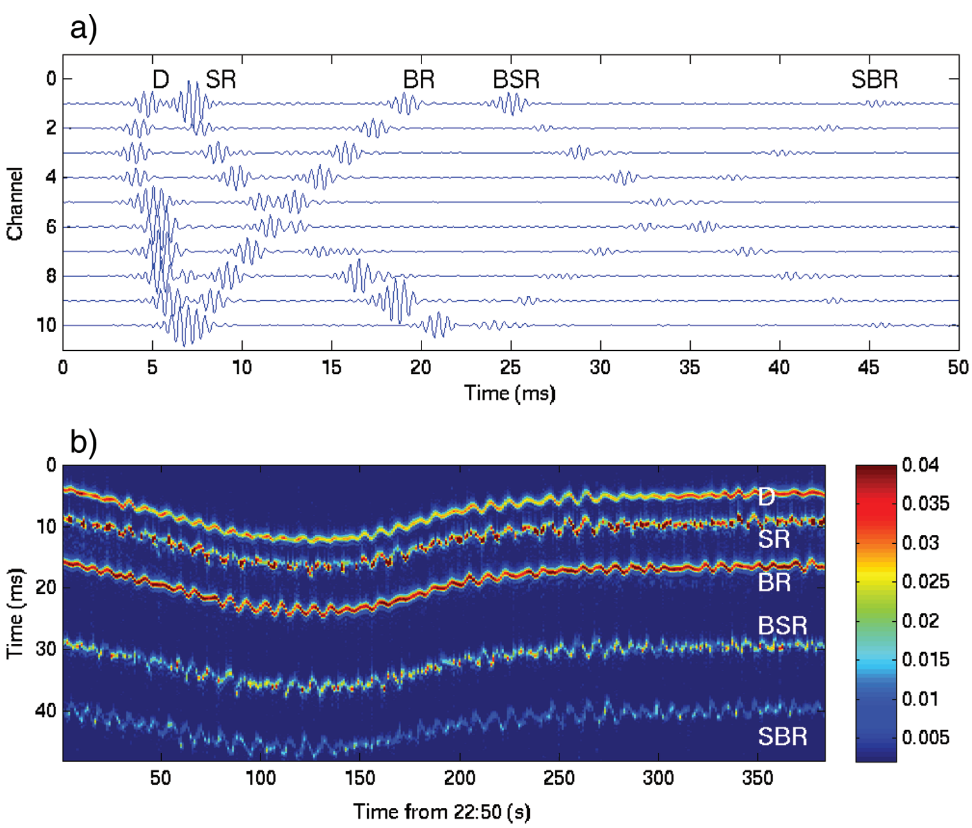

FIG. 2. (Color online) Matched filtered acoustic data (a) on the VLA at 22:50 UTC and (b) on channel 3 for 380 pings starting at 22:50 UTC (D, direct; SR, surface reflected; BR, bottom reflected; BSR, bottom–surface reflected; and SBR, surface–bottom reflected arrival). In (b) the matched filtered envelope amplitude is color coded (arbitrary units).

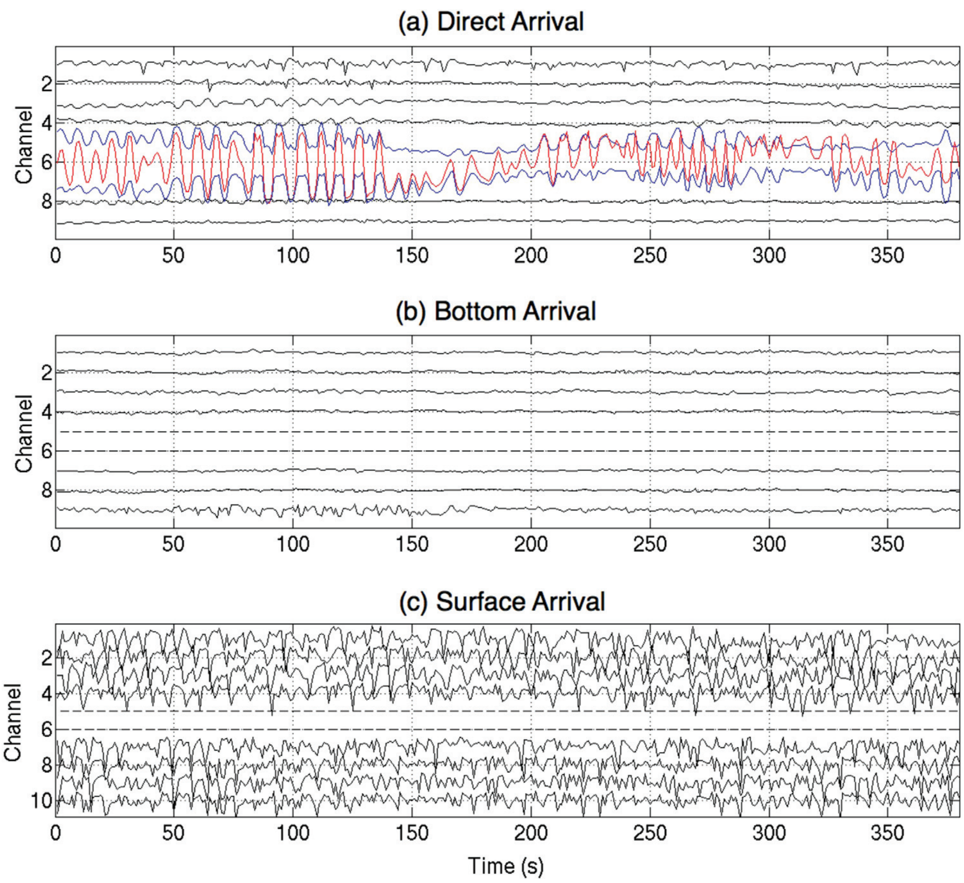

FIG. 3. (Color online) Amplitude time series of the maximum of envelopes of (a) D, (b) BR, and (c) SR arrival for 380 pings starting at 22:50 UTC. A few arrivals overlap [see Fig. 2(a)] and are not shown: D and BR arrivals for channel 10, and BR and SR arrivals for channels 5 and 6.

arrival-time fluctuations for the five arrivals show a period that could correspond to ocean surface waves. The surface-reflected arrivals (SR, SBR, and BSR) show significant amplitude fluctuations.

To obtain high-resolution arrival time and amplitude, the data were up-sampled by a factor of four to 25 kHz. From the up-sampled matched filtered time series, the maximum of the envelope of amplitudes of the direct, surface-, and bottom-reflected arrivals were estimated using a wavelet matching technique. For all channels, the amplitudes shown in Fig. 3 of (a) D, (b) BR, and (c) SR arrivals were extracted from 380 pings (called "amplitude time series"). The direct arrival shows strong amplitude fluctuation where the fluctuation is most severe in channels 5–7, located just below the strong thermocline. The SR arrivals are fluctuating for all receiver depths and the BR arrivals are stable except for channels 5 and 6, due to the interference of SR and BR signals [see Fig. 2(a)].

The amplitude time series of the D, BR, and SR arrivals on channel 3 are shown in the left column of Fig. 4 with corresponding spectrograms in the right column of Fig. 4. For the spectrograms, a 64-point (64 s) fast Fourier transform (FFT) was applied to the amplitude time series. Each snapshot was advanced 32 s, but no averaging was performed.

In the D arrival [Fig. 4(a)], abrupt amplitude variations are observed irregularly. In addition, a persistent fluctuation of smaller amplitude is seen in most parts of the time series. Significant change of the water column SSP causes variations in ray arrivals. Rays propagating at shallow grazing angles, as the direct arrivals, are more influenced by the SSP with a thermocline [Fig. 1(b)]. One component of the SSP change is due to the significant internal wave activity at the experiment site.[9–11] An interesting feature is the persistent fluctuation in the D arrivals. According to the spectrogram of the direct arrivals [Fig. 4(b)], the fluctuation is around 0.12 Hz, which agrees with the peak of the ocean surface wave spectrum [see Fig. 1(c)]. A fluctuation at the same frequency is also observed in the BR arrival spectrogram [Fig. 4(d)], although the amplitude time series [Fig. 4(c)] is more stable than the other two arrivals.

The amplitude time series for the SR arrivals [Fig. 4(e)] shows a noise-like behavior but its spectrogram [Fig. 4(f)] is dispersed between 0.1 and 0.2 Hz and faint sinusoidal variation in the spectrogram structure can be observed. The randomness of the SR arrivals comes from the scattering from the irregular ocean surface boundary. Shallow water sound propagation across the crest of irregular surface wave has been modeled in Ref. 12, but modeling along the crests has not yet been performed. Noting that the dominant wave direction is 90°, we speculate that the faint sinusoidal variation in spectrogram structure is due to propagation differences in response for acoustic waves in the along and across ocean wave direction.

Spectral analysis of the arrival amplitudes shows that the fluctuations are related to ocean surface waves. To quantify the effect of surface waves, a statistical analysis with respect to receiver depth was carried out using amplitudes over a 1 min period rather than the entire observation period (this reduces the effect of radial source array variation). Figure 5(a)

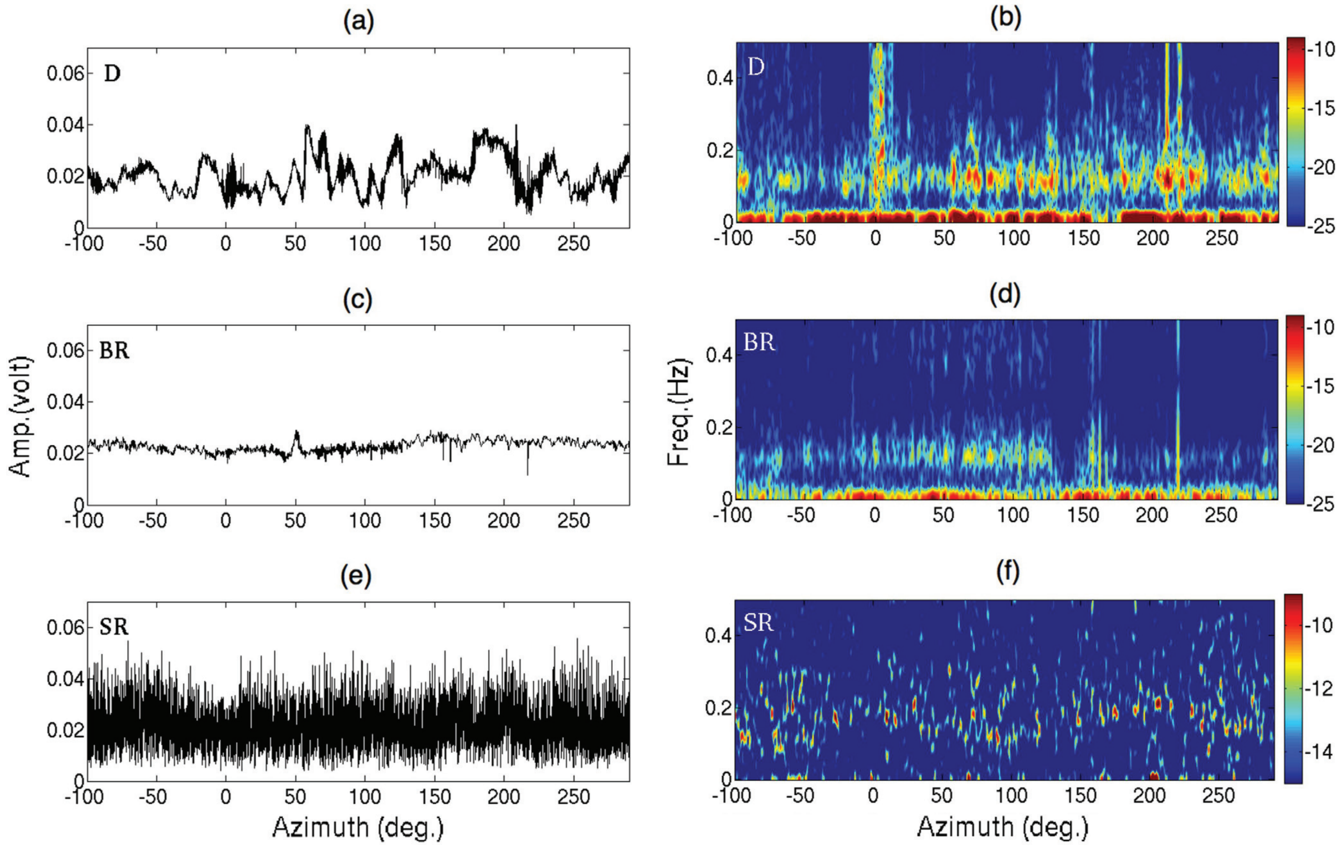

FIG. 4. (Color online) Amplitude time series (left column) and spectrograms (right column) of D [(a) and (b)], BR [(c) and (d)], and SR [(e) and (f)] arrivals over entire circle for channel 3. The horizontal axis is the source–VLA azimuth [see Fig. 1(a)]. The dynamic range of (f) differs from (b) and (d) for a more clear representation.

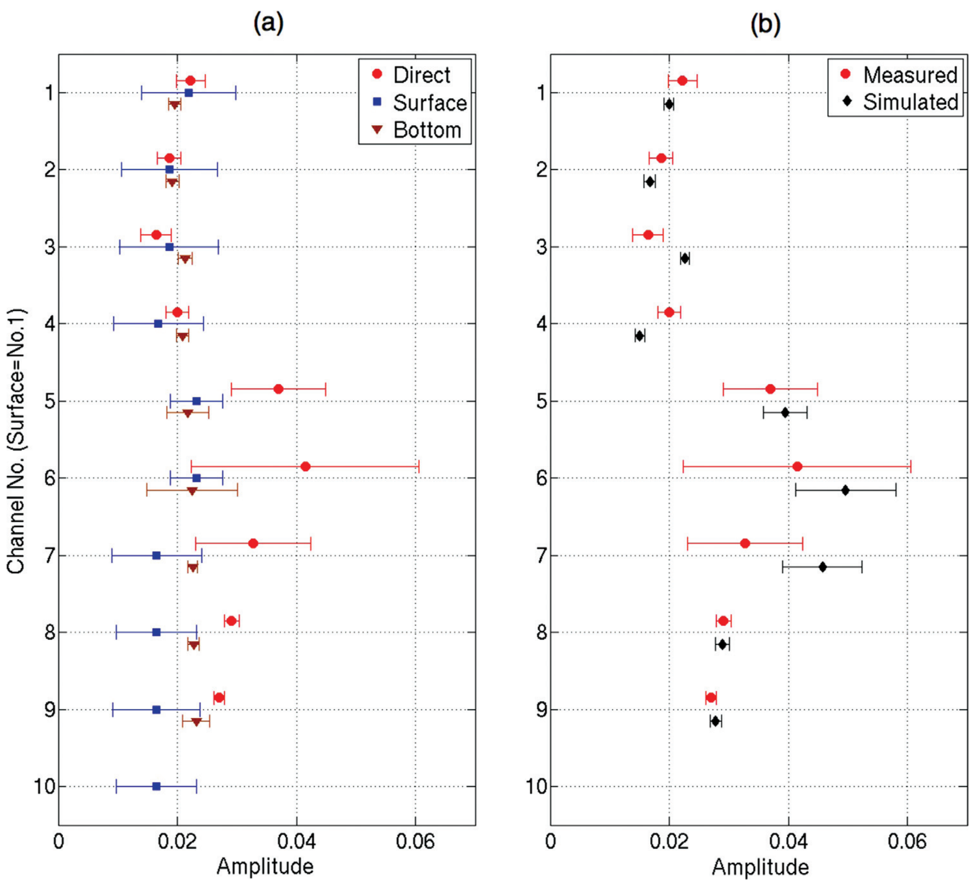

FIG. 5. (Color online) Amplitude variations for (a) measured D, SR, and BR arrivals for 1 min duration starting at 22:50 UTC and (b) measured and simulated (normalized) direct arrivals. The symbols represent the mean value and the horizontal bar twice the standard deviation. Due to overlapping signals the following arrivals are not shown: BR and SR for channels 5 and 6 and the direct and bottom-reflected for channel 10. For the simulation, the SSP was constant while the source oscillated vertically between 34 and 36 m with frequency 0.12 Hz.

shows these statistics for amplitudes of the D, SR, and BR arrivals for 60 pings (1 min) starting at 22:50 UTC.

The SR arrivals show large amplitude fluctuations for all receiver depths with mean amplitude slowly increasing with depth (longer ray path). The BR arrivals have the smallest standard deviation among the three kinds of arrivals. The overall mean amplitudes of SR arrivals are smaller than those of BR arrivals. This is in contrast with the ideal flat surface and bottom boundaries. Thus, this could be due to scattering from surface waves.

The direct arrivals show a depth-dependent feature that is distinguished from other arrivals. At first, large amplitude fluctuations are observed at the hydrophones located in the middle of the water column where the acoustic propagation is most influenced by the negative gradient thermocline [see Fig. 1(b)] for the given source–receiver configuration. Second, small mean amplitudes of direct arrivals are observed in the upper three channels (channels 1–3) compared with the other channels, which cannot be explained by simple geometrical spreading.

The most obvious influence of ocean surface waves on the experiment is to cause ship motion that accompanies movement of the source attached to the towing ship. The source will oscillate at the surface wave frequency and its amplitude will be determined by the coupled heaving and pitching ship motion.[13,14] In our case, the significant wave height of the ocean was approximately 2.2 m, and considering the pitch motion to be small, the source oscillation amplitude would be within 1–3 m. Although ocean surface waves can cause variation in the SSP due to water particle motion, the motion decreases exponentially with depth and practically can be ignored. Thus, it is assumed that the relative vertical motion between the source and the thermocline oscillates with amplitude within 1–3 m.

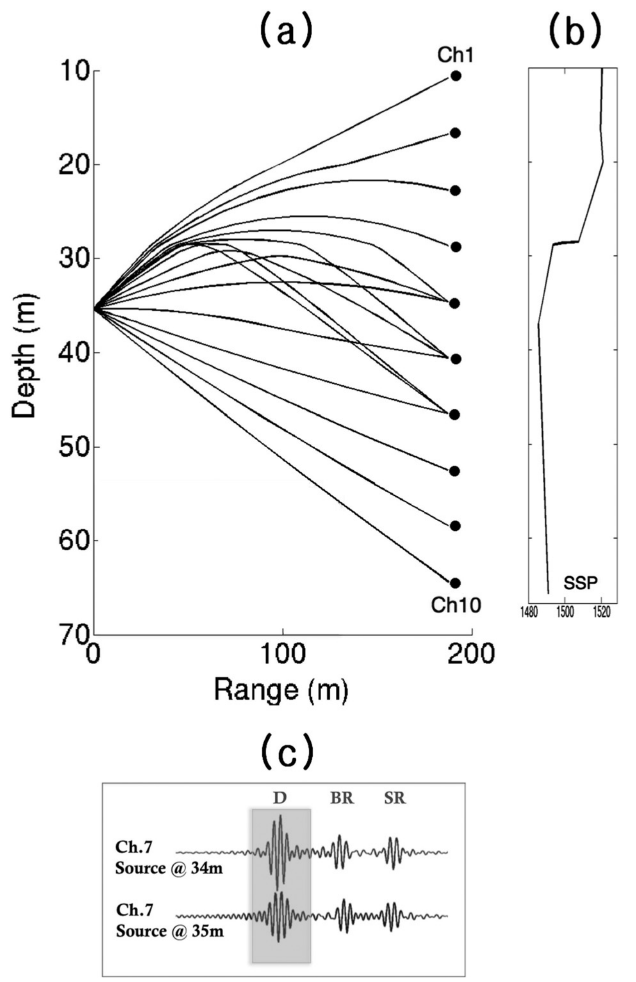

FIG. 6. (a) Ray path diagram of the direct arrival for the source depth of 35 m. (b) The SSP used in the simulation. (c) Simulated signals at 34 and 35 m source depths.

B. Simulation of the direct arrival amplitude fluctuations

Focusing on the D arrivals, a simulation was performed to test if the thermocline along with the source oscillation reproduces the observed features in the water column (see Fig. 5). For the simulation, the SSP of Fig. 6(b) was used. The SSP was inverted using the approach in Ref. 3 and the data were measured at 22:50 UTC. The SSP was held constant while the source oscillated between 34 and 36 m at the frequency 0.12 Hz.

Figure 5(b) shows the simulation results compared with the measured results for the direct arrival [Fig. 5(a)]. The simulation produced D arrival features similar to those in the observations. A large amplitude and amplitude-variation at channels 5–7 are observed. The ray path diagram in Fig. 6(a) of the direct arrival for the 35 m source depth using the SSP in the right panel shows multiple eigenrays at just below the strong thermocline. The number of eigenrays and their interference varies with the source depth. The influence of the thermocline on ray propagation is most significant for the D arrival [see Fig. 6(c)]. Thus the significant amplitude fluctuation of direct arrivals at some receivers below the thermocline is due to the interference of multiple direct path eigenrays.

Small amplitudes are observed for the direct arrivals above the thermocline (channels 1–4) in Fig. 5. As an acoustic wave propagates from the source, the energy is confined in a ray tube. In an isovelocity medium, the ray paths are straight and the amplitude depends only on the travel length (geometrical spreading). In a refracting medium, however, the ray tube cross-section and thus the resulting arrival amplitude depend on the refraction over the ray path following Snell's law.[15] Above the thermocline, the eigenrays experiences larger ray tube expansion than simple geometric spreading while passing through the thermocline zone at low grazing angle. Thus, the direct path amplitudes are lower in the upper channels in Fig. 5.

IV. CONCLUSION

Fluctuating received array signals have been analyzed so they can be used appropriately for geoacoustic inversion. Significant fluctuations in the D and SR arrivals of short-range chirp transmissions (1.1–2.9 kHz) were observed from the SWAMI32 circle event (radius 198 m) of the SW06 experiment. The dominant frequency of the arrival fluctuations coincides with the peak frequency of ocean surface waves (0.12 Hz) and the fluctuations below the strong thermocline were largest for the direct arrivals. Similar fluctuations were simulated for a sound speed profile with a strong thermocline and a vertically oscillating source due to ocean surface waves.

ACKNOWLEDGMENT

The authors are grateful to D. Knobles for providing the SWAMI32 data. This work was supported by Office of Naval Research Grant No. N00014-05-1-0264, Korea Research Foundation Grant No. KRF-2009-013-D00139, and KORDI Grant No. PES132B.

[1]D. J. Tang, J. Moum, J. Lynch, P. Abbot, R. Chapman, P. Dahl, T. Duda, G. Gawarkiewicz, S. Glenn, J. Goff, H. Graber, J. Kemp, A. Maffei, J. Nash, and A. Newhall, "Shallow Water '06—A joint acoustic propagation/nonlinear internal wave physics experiment," Oceanogr. **20**(4), 156–167 (2007).
[2]Y.-M. Jiang, N. R. Chapman, and P. Gerstoft, "Short range geoacoustic inversion with vertical line array," J. Acoust. Soc. Am. **124**(3), EL135–EL140 (2008).
[3]C. Park, W. Seong, P. Gerstoft, and W. S. Hodgkiss, "Geoacoustic inversion using back-propagation," IEEE J. Oceanic Eng., In Press.
[4]Y.-M. Jiang and N. R. Chapman, "Estimating geoacoustic properties of marine sediment on the New Jersey continental shelf from broadband signals," J. Acoust. Soc. Am. **126**(4), 2316 (2009).
[5]D. P. Knobles, P. S. Wilson, J. A. Goff, and S. E. Cho, "Seabed acoustics of a sand ridge on the New Jersey continental shelf," J. Acoust. Soc. Am. **124**(3), EL151–EL156 (2008).
[6]T. A. Davies, J. A. Austin, Jr., M. B. Lagoe, and J. D. Milliman, "Late Quaternary sedimentation off New Jersey: New results using 3-D seismic profiles and cores," Mar. Geol. **108**, 322–343 (1992).
[7]H. C. Graber, E. A. Terray, M. A. Donelan, W. M. Drennan, J. C. Van Leer, and D. B. Peters, "ASIS—A new air-sea interaction spar buoy: Design and performance at sea," J. Atmos. Ocean. Tech. **17**, 708–720 (2000).
[8]H. O. Berteaux, *Buoy Engineering* (Wiley Interscience, New York, 1976), Chap. 2.
[9]J. Luo, M. Badiey, E. A. Karjadl, B. Katsnelson, A. Tskholdze, J. F. Lynch, and J. N. Moum, "Observation of sound focusing and defocusing due to propagating nonlinear internal waves," J. Acoust. Soc. Am. **124**(3), EL66–EL72 (2008).
[10]D. Rouseff, D. Tang, K. L. Williams, Z. Wang, and J. N. Moum, "Mid-frequency sound propagation through internal waves at short range with synoptic oceanographic observations," J. Acoust. Soc. Am. **124**(3), EL73–EL77 (2008).
[11]B. Katsnelson, V. Grigorev, and J. F. Lynch, "Intensity fluctuations of midfrequency sound signals passing through moving nonlinear internal waves," J. Acoust. Soc. Am. **124**(3), EL78–EL84 (2008).
[12]C. T. Tindle and G. B. Deane, "Shallow water sound propagation with surface waves," J. Acoust. Soc. Am. **117**(5), 2783–2794 (2005).
[13]E. V. Lewis, *Principles of Naval Architecture: Motions in Waves and Controllability* (SNAME, Jersey City, 1988), Part 2.
[14]R. G. Dean and R. A. Dalrymple, *Water Wave Mechanics for Engineers and Scientists* (World Scientific, New York, 1990), Chap. 4.
[15]H. Medwin and C. S. Clay, *Fundamentals of Acoustical Oceanography* (Academic Press, New York, 1997), Chap. 2.